Electrochimica Acta 509 (2025) 145302

Contents lists available at ScienceDirect

Electrochimica Acta

journal homepage: www.journals.elsevier.com/electrochimica-acta

Aqueous solution-based synthesis approach for carbon-disordered rocksalt composite cathode development and its limitations

Venkata Sai Avvaru [a], Mateusz Zuba [b], Beth L. Armstrong [c], Shilong Wang [a,d], Dong-Min Kim [e], Isik Su Buyuker [b], Carrie Siu [b], Brett A Helms [a,e], Ozgenur Kahvecioglu [b], Haegyeom Kim [a,*]

[a] Materials Sciences Division, Lawrence Berkeley National Laboratory, Berkeley 94720, CA USA
[b] Applied Materials Division, Argonne National Laboratory, Lemont 60439, IL USA
[c] Materials Science and Technology Division, Oak Ridge National Laboratory, Oak Ridge 37831, TN, USA
[d] Department of Materials Science and Engineering, UC Berkeley, Berkeley 94720, CA, USA
[e] Molecular Foundry Division, Lawrence Berkeley National Laboratory, Berkeley 94720, CA USA

ARTICLE INFO

Keywords:
Cathodes
Disordered rock-salt
Lithium-ion batteries
Carbon composite
Aqueous synthesis
Dissolution

ABSTRACT

Disordered rocksalt cathodes exhibit high specific capacities and high energy density; however, their low electronic conductivity poses a great challenge. Herein, we explored an aqueous-solution-based synthesis route that involves controlling the surface charges of $Li_{1.2}Mn_{0.6}Ti_{0.2}O_{1.8}F_{0.2}$ (LMTOF) to be anchored by a few-layer reduced graphene oxide (rGO) for the first time. The uniform rGO wrapping on the surface of the LMTOF particles is achieved by electrostatic attraction between the negatively charged rGO and positively charged LMTOF particles. Although the initial specific capacity of rGO-LMTOF composite increased by 58 % compared to the pristine LMTOF, the composite experienced a severe capacity fade over cycling. The synthesis process in an aqueous medium resulted in Li^+/H^+ exchange and TM dissolution as evidenced from inductively coupled plasmon analysis and X-ray diffraction analysis. Therefore, this work suggests the search for alternative media or conditions for the synthesis of carbon-disordered rock salt cathode composite.

1. Introduction

Disordered rocksalt with lithium excess (DRX) compounds have emerged as low-cost and high-capacity (> 250 mAh/g) cathode materials for lithium-ion batteries (LIBs). [1–6] Whereas conventional ordered layered oxide cathode materials for LIBs rely on the use of cobalt (Co) and/or nickel (Ni). [7,8] DRX compounds enable the use of various transition metals (TMs), providing additional flexibility. This is possible because the requirement of Li/TM separation in the crystal structure is lifted, [9] enabling the development of cathode materials based on abundant and inexpensive TMs such as manganese (Mn) and iron (Fe). [10–13] In addition, because DRX compounds can use both cationic and anionic redox reactions, their achievable specific capacity is not limited by the available cationic redox reactions of the TM; these materials can thus deliver high specific capacity exceeding 250 mAh/g. [14–16]

Despite recent significant improvements, DRX cathode development remains in its infancy, and several important challenges remain before they become practically viable and competitive with commercially available ordered layered oxide cathodes. One significant issue is their relatively low electronic conductivity. [16–18] Most studies on DRX cathode materials have used a relatively high carbon content (≥ 20 wt %) in the electrode preparation, [19,20] which greatly decreases the electrode-level energy density. In addition, most DRX cathode studies use high-energy ball milling to reduce the particle size of the DRX and create homogeneous carbon mixing with DRX particles. [21,22] However, this process is not suitable for scale-up. Patil et al. recently developed a graphitic carbon coating on a DRX surface and demonstrated improved cycling stability with a relatively low carbon content (10 wt%); however, the high-energy ball-milling process was still used. [17] A vapor-phase carbon-coating method was applied to the DRX-type $Li_{1.2}Mn_{0.4}Ti_{0.4}O_2$ compound by Xu et al.; however, only a limited reversible capacity of 70 mAh/g was achieved without additional high-energy ball milling with carbon nanotubes. [22] Although graphitic carbon coating is preferred because non-graphitic carbon with substantial defects accelerates the electrolyte decomposition and degrades the cathode performance, [23] graphitic carbon coating typically requires high-temperature treatment at reducing environments that can decompose the DRX-type compounds. [22]

* Corresponding author.
E-mail address: haegyumkim@lbl.gov (H. Kim).

https://doi.org/10.1016/j.electacta.2024.145302
Received 13 August 2024; Received in revised form 21 October 2024; Accepted 30 October 2024
Available online 30 October 2024

In this study, we explore a solution-based synthesis route that uses the electrostatic interaction between $Li_{1.2}Mn_{0.6}Ti_{0.2}O_{1.8}F_{0.2}$ (hereafter, LMTOF) particles and few-layer reduced graphene oxide (rGO) sheets by controlling the surface charges of LMTOF for the first time. Although we confirm that the rGO sheets wrap the LMTOF particles, the synthesis process in aqueous medium resulted in the leaching of metal ions and Li^+/H^+ exchange, as evidenced from inductive coupled plasmon (ICP) analysis and X-ray diffraction (XRD) analysis, which remains a limitation.

2. Experimental section

2.1. Material synthesis

Reduced graphene oxide (rGO)-wrapped LMTOF particles were prepared through a simple one-step process. Initially, LMTOF was prepared *via* solid-state synthesis following a previously reported synthesis method. [24] Typically, Mn_2O_3, TiO_2, Li_2CO_3, and LiF precursors adding up to ~200 g was ball-milled together with Y-stabilized ZrO_2 in 500-mL jars at 100 rpm using a Retsch Planetary Ball Mill PM 400. The milled precursors were calcined at 1000 °C for 4 h using a ramp rate of 5 ℃ min^{-1} under an argon (Ar) atmosphere. Calcination was conducted in loose powder form at a 30-g scale. The calcined LMTOF was subsequently ball-milled at 400 rpm in an organic solvent for 4 h without any carbon. The ball-milled material was recovered, dried, and sieved using 45-micron mesh. All the processes were conducted at the Materials Engineering Research Facility at Argonne National Laboratory (ANL).

For the rGO wrapping, 20 wt% of graphite oxide (~20 μm, MSE supplies) was dispersed in deionized water (0.2 mg mL^{-1}) and exfoliated to graphene oxide by sonication for 100 min. The graphene oxide was reduced by slowly adding 0.15 M of urea (99.9 % Sigma-Aldrich) to the solution followed by stirring for 10 h at 80 °C in an oil bath. Next, 80 wt % of the LMTOF powder was added to the above solution, and the solution was stirred for 1 h at room temperature. Finally, the pH of the solution was adjusted to 2, where the LMTOF and rGO have opposite surface charges. rGO-wrapped LMTOF particles were obtained by washing the resultant products using distilled water followed by drying at 70 °C. rGO-wrapped PEI-coated LMTOF (hereafter, GPLMTOF) particles were prepared using a two-step process involving (1) coating of LMTOF particles by a polyethylenimine (PEI) and (2) wrapping the polymer-coated LMTOF particles in rGO sheets. In a typical process, 1 g PEI and 0.8 g polyvinylpyrrolidone (PVP) were dissolved in 20 mL of ethanol and methanol (1:1) mixture solution; subsequently, 1 g LMTOF was dispersed in the solution at a concentration of 50 mg/mL. The dispersion was subjected to sonication for 60 min and stirred at 600 rpm for 24 h at room temperature. PEI-coated LMTOF (hereafter, PLMTOF) was obtained by washing the products using methanol and acetone followed by drying at 70 °C. For the GPLMTOF, 20 wt% of graphite oxide was exfoliated to graphene oxide using sonication and it was reduced by urea, following a similar procedure mentioned above. Then, 80 wt% of PEI-coated LMTOF powder was added to the solution, and the solution was stirred for 1 h at room temperature at a neutral pH. The resultant sample was washed with distilled water followed by drying at 70 °C. Finally, the rGO-wrapped PEI-coated LMTOF was heat treated at different temperatures ranging from 200 °C to 300 °C under Ar flow for 2 h to remove the additional functional groups (heating rate of 5 °C min^{-1}).

2.2. Materials characterization

The zeta potential was collected on a Brookhaven ZetaPALS instrument. Samples were prepared by making a stock solution of powder @ 10^{-3} concentration in 5 mL of 1 mM KNO_3. Seven aliquots were prepared from this stock solution using 40 μL of the stock solution into 20 ml of 1 mM KNO_3, and either the pH was recorded as is or each solution was adjusted with nitric acid or ammonium hydroxide to achieve a desired pH, ranging from pH 2 to pH 10. The zeta potential was subsequently measured, with each measurement being the average of 100 cycles.

A Rigaku Miniflex 600 high-resolution diffractometer equipped with a Cu-Kα source (λ=0.15418 nm) was used for recording the XRD patterns of the LMTOF-based samples.

Microstructural analysis of LMTOF samples was conducting using a FEI Quanta FEG-250 and Phenom PW-100–017 scanning electron microscope. Energy-dispersive X-ray spectroscopy (EDS) elemental mappings were recorded using a Bruker Quantax EDS detector.

Inductively coupled plasma mass spectroscopy (ICP-MS; Agilent 7900) was used to investigate the ratio of elements present in the processing solution. For this measurement, 20 mg of LMTOF was dispersed in 20 mL of the solvent, and the suspension was left for different time intervals. For the analysis, 20 μL of the solution was collected after filtering out the LMTOF and then diluted with nitric acid for the ICP-MS. The calibration curve was generated using standard solutions with 5 different concentrations ranging from 1 ppb to 1000 ppb. Linear fitting was applied.

The carbon content of the GPLMTOF sample was measured using TGA (TGA5500, TA Instruments). The measurement was performed at a heating rate of 1 ℃ min^{-1} from room temperature to 650 ℃ using an aluminum pan.

2.3. Electrochemical study

GPLMTOF composite electrodes were prepared by hand mixing 80 wt% GPLMTOF with 10 wt% super C65 (Timcal) and 10 wt% of polytetrafluoroethylene (PTFE, DuPont, Teflon 8A). For the control group, the electrode was prepared by mixing 70 wt% of LMTOF, 20 wt% of super C65, and 10 wt% of PTFE binder. The mixtures were then rolled into a ~40-μm thin film inside an Ar-filled glovebox. Coin-type 2032 two-electrode cells were fabricated using the composite working electrode (10 mm diameter) containing ~2.8 mg cm^{-2} of the active material, Li-foil counter/ reference electrode and a glass fiber separator (Whatman, GF/B type). The electrolyte consists of a 1 M solution (99.99 %, Solvionic) of $LiPF_6$ in a 1:1 mixture of ethylene carbonate (EC) and dimethyl carbonate (DMC). A glove box (VAC) filled with high-purity argon (99.999 %) and equipped with oxygen and moisture sensors/absorbers (H_2O and O_2 content < 1 ppm) was used for assembling the electrochemical cells. Li-ion half-cells were subjected to galvanostatic long-term cycling at 20 mA g^{-1} in the voltage range of 4.8–2 V using an Arbin battery testing instrument at room temperature.

3. Results and discussion

3.1. LMTOF-graphene composite synthesis in acidic environments

In this study, LMTOF powder was synthesized using a conventional solid-state method following a previous study. [24] We selected this specific LMTOF material as a model system for rGO composite development because it can be synthesized at large-scale and has shown reasonably good electrochemical performance. [3,24] The rGO-wrapped LMTOF was synthesized using a solution-based synthesis route that utilizes an electrostatic interaction between LMTOF particles and few-layer rGO sheets, similar to the use of a rGO coating on $Li_4Ti_5O_{12}$ in our previous work. [25] Herein, we selected aqueous medium as a processing solvent because rGO sheet is known to be well dispersed in it [26] and because of its expected low environmental impact. Initially, the surface charges of the LMTOF particles and graphene oxide were determined from Zeta potential measurements. Fig. 1a presents the measured Zeta potential of the LMTOF at varied pH levels. The LMTOF particles held positive surface charges at pH 2, whereas they held negative surface charges at higher pH. Because graphene oxide has a negative charge across a wide range of pH levels between 2 and 12, [25] the negatively charged rGO sheets may electrostatically attract

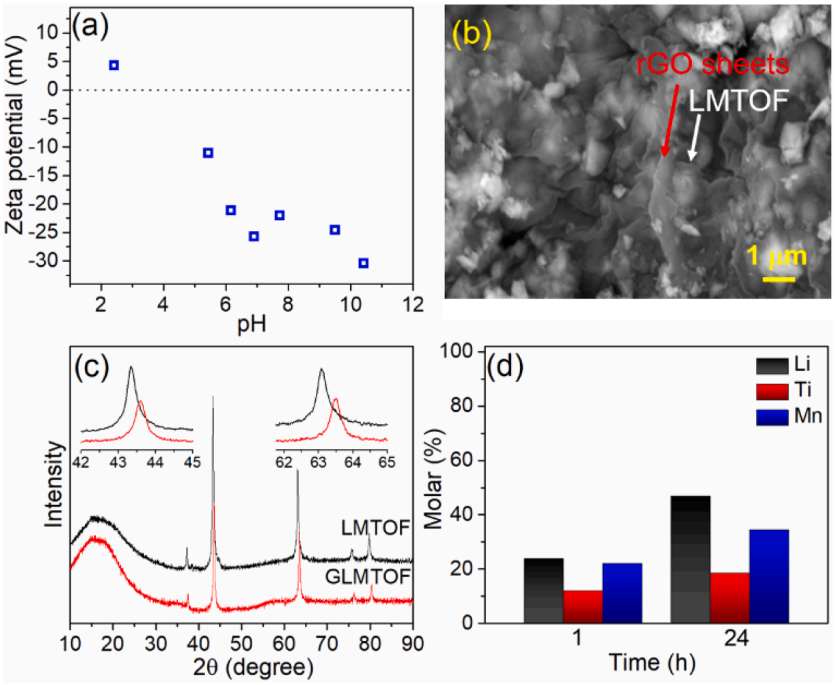

Fig. 1. (a) Zeta potential of LMTOF at various pH, (b) SEM image of rGO-wrapped LMTOF (GLMTOF), (c) XRD patterns of LMTOF and GLMTOF, and (d) ICP-MS analysis of the solutions collected at different time intervals after LMTOF powders were dispersed in water at pH 2.

positively charged DRX particles at pH 2, resulting in the rGO wrapping over LMTOF (GLMTOF) particles. Fig. 1b presents a scanning electron microscopy (SEM) image of the GLMTOF sample, which confirms the uniform wrapping of rGO sheets on submicron LMTOF particles.

To understand whether the bulk structure of LMTOF is changed after the solution-based synthesis process, we employed XRD analysis, as shown in Fig. 1c. The XRD peaks of GLMTOF shifted to higher two-theta angles compared with those of the pristine LMTOF sample; however, no secondary impurity peaks were detected. We suspect the occurrence of Li leaching out from the LMTOF during the solution-based synthesis process because of the acidic environment. Fig. 1d presents the inductively coupled plasma mass spectroscopy (ICP-MS) analysis of the solution collected at different time intervals from the suspension of LMTOF at pH 2. The ICP-MS analysis demonstrated that not only Li ions but also Mn and Ti ions are leached out of the LMTOF powder. After 1 h of immersion in pH 2 solvent, >23 % of the Li was leached out from the LMTOF (0.27 Li out of 1.2 Li) and 20 % of Mn (0.12 Mn out of 0.6 Mn) and 11 % of Ti (0.022 Ti out of 0.2 Ti) were leached out from the LMTOF. The leaching of Li, Mn, and Ti from LMTOF became more significant after 24 h of immersion in the pH 2 solvent. These results demonstrate that the dissolution of Li, Mn, and Ti occurs, accompanied by structure change during the solution-based synthesis process of GLMTOF at pH 2 in an aqueous medium while superior wrapping of rGO on LMTOF particles is feasible. It is possible that impurities such as Li_2CO_3 (if any) can contribute to the Li dissolution in the pH2 solution, but we do not expect its contribution would be substantial because we did not observe a noticeable amount of Li_2CO_3 or other impurities in the XRD analysis.

3.2. LMTOF-graphene composite synthesis in neutral environments

Another approach for rGO wrapping at neutral pH is proposed in this work and involves a two-step process: (1) coating of LMTOF particles by polyethyleneimine (PEI), which carries a positive surface charge, [27] followed by (2) wrapping the polymer-coated LMTOF particles with negatively charged rGO sheets. The morphology and structure of LMTOF were observed to remain intact after the PEI coating, as evidenced by the SEM and XRD analysis (Figures S1a–b). In addition, the electrochemical performance of LMTOF did not significantly change after PEI coating (Figure S1c). The GPLMTOF was obtained by exfoliating graphite oxide to graphene oxide using sonication and then reducing it by urea followed by the addition of PEI-coated LMTOF (see details in experimental section). Figs. 2a and 2b show SEM images of the pristine LMTOF and GPLMTOF samples, respectively. Fig. 2b clearly shows that most of the LMTOF particles were wrapped by two-dimensional rGO sheets in contrast to the pristine LMTOF particles in Fig. 2a. Energy-dispersive X-ray spectroscopy (EDS) analysis further confirmed the uniform coverage of carbon on LMTOF particles in Fig. 2d. In contrast, no C signal was observed in LMTOF particles without rGO wrapping (Fig. 2c). The carbon signal shown in the background of Fig. 2c comes from the carbon tape that is used to hold LMTOF particles on the SEM sample holder. Figure S2 presents the thermogravimetric analysis result for the GPLMTOF, which was conducted in an oxygen atmosphere to estimate the carbon content. The GPLMTOF sample experienced a weight loss of 21 % in the temperature range of 30 °C–650 °C, indicating approximately 21 wt% of total carbon content presents in the composite. Fig. 2e shows the XRD patterns of LMTOF, PLMTOF, and GPLMTOF. No significant secondary phases were detected in the XRD patterns after PEI coating and rGO wrapping. Although a slight peak shift and peak broadening at ~63° were observed after rGO wrapping, it is noteworthy that the XRD peak shift detected for GPLMTOF is not significant, as observed at pH 2 in Fig. 1c, which might indicate improved stability of LMTOF in a neutral aqueous medium compared with that in an acidic environment at pH 2.

3.3. Electrochemical performance evaluation of LMTOF-graphene composite

To reduce the total rGO content in the composite, we also synthesized GPLMTOF with reduced rGO content (~10 wt%). We confirmed that the rGO wrapping over PLMTOF was achieved with ~10 wt% carbon, as evidenced from the SEM image presented in Figure S3. The carbon content in this GPLMTOF composite was estimated from a carbon analyzer. The 10 wt%-rGO-wrapped PLMTOF (namely 10GPLMTOF) was used for the electrochemical tests. The

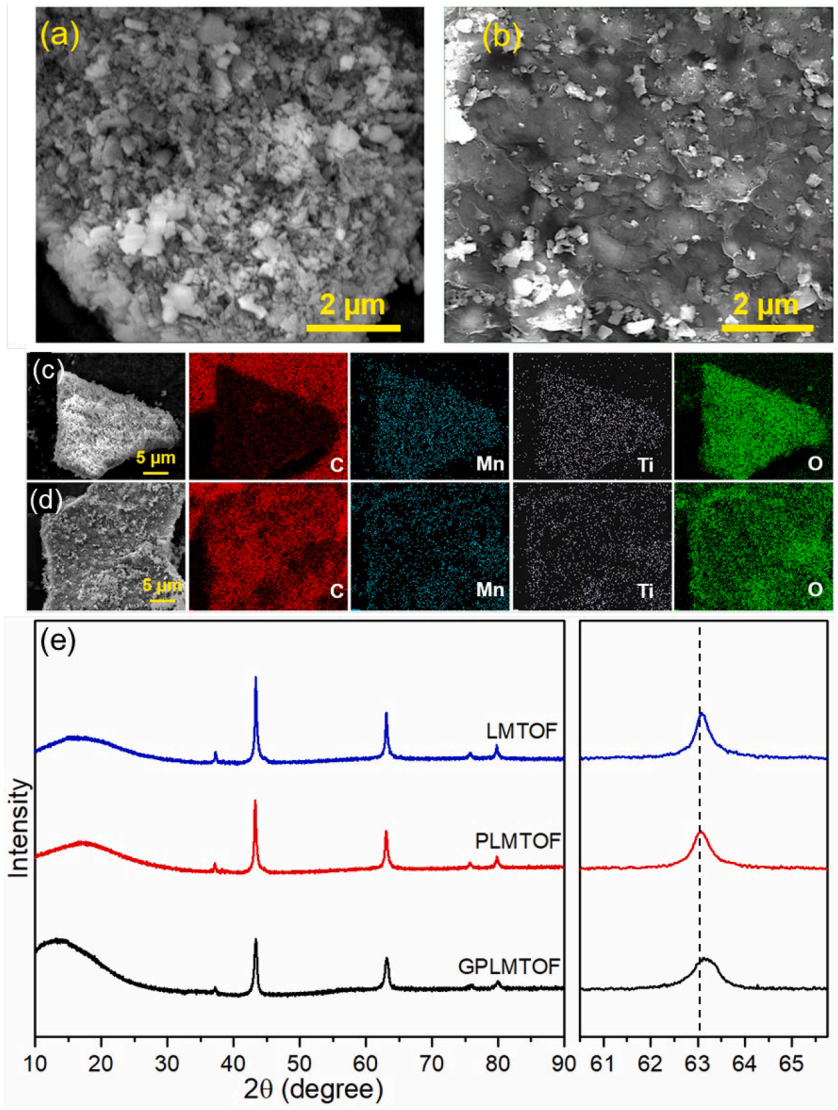

Fig. 2. SEM images of (a) LMTOF and (b) GPLMTOF. SEM images and EDS mapping results of (c) LMTOF and (d) GPLMTOF. (e) XRD of LMTOF, PLMTOF and GPLMTOF.

electrochemical performance of 10GPLMTOF was investigated in Li-metal half-cells. Figs. 3a and 3b present the galvanostatic charge–discharge profiles of the pristine LMTOF and 10GPLMTOF at 20 mA/g in the voltage range of 4.8–2.0 V (*vs.* Li/Li^+). LMTOF exhibits the characteristic behavior of DRX materials with an initial discharge capacity of 168 mAh/g at a current density of 20 mA/g, retaining 152 mAh/g after 50 cycles (Fig. 3a). [2] In contrast, 10GPLMTOF exhibits a high initial discharge capacity of 266 mAh/g at 20 mA/g with significantly improved initial coulombic efficiency (160 % *vs.* 59 % of LMTOF). It is possible that the rGO wrapping suppresses the irreversible side reactions; however, we cannot exclude the possibility of Li loss during the synthesis process. Fig. 3c shows the cycling stability of the LMTOF and 10GPLMTOF electrodes. Although the initial discharge capacity of the 10GPLMTOF composite was higher than that of LMTOF, faster capacity fade was observed in 10GPLMTOF over extended cycling, with retention of ~47 % of the initial capacity after 50 cycles compared to 90 % for LMTOF.

The pristine LMTOF shows relatively good capacity retention as mentioned earlier, but a voltage decay during discharge is observed in Fig. 3a. To better capture this behavior, we plotted the average charge and discharge voltages of LMTOF and 10GPLMTOF at 20 mA/g as shown in Fig. 3d. The pristine LMTOF shows a continuous decrease in both average discharge and charge voltages while the voltage decrease in discharging process is more obvious, indicating a continuous structural change during repeated charge-discharge processes. [28] In contrast, the average discharge voltage of 10GPLMTOF decreases while there is a slight increase in charge voltages upon cycling at 20 mA/g. These voltage changes may reflect a polarization increase due to various factors including electrolyte decomposition and Mn dissolution during cycling. [29] The increase in polarization in 10GPLMTOF during cycling is likely to lead to rapid capacity decay compared to LMTOF. The capacity decay observed in 10GPLMTOF could be related to the presence of residual functional groups in the rGO [30,31] because the functional groups in rGO decrease electrical conductivity and have catalytic effects, which might accelerate electrolyte decomposition. [32]

Therefore, the 10GPLMTOF composite was heat-treated at different temperatures ranging from 200 °C to 300 °C to remove the residual functional groups. Fig. 4a shows the XRD patterns of 10GPLMTOF heat treated at 200 °C (denoted as 10GPLMTOF200), 250 °C (denoted as 10GPLMTOF250) and 300 °C (denoted as 10GPLMTOF300) as well as pristine LMTOF. We found that the broad secondary peaks evolved at 18°, ~36° and ~58° in the 10GPLMTOF composites after the heat treatment that correspond to the spinel-like phase. This spinel-like secondary phase is more prominent in the case of 10GPLMTOF300

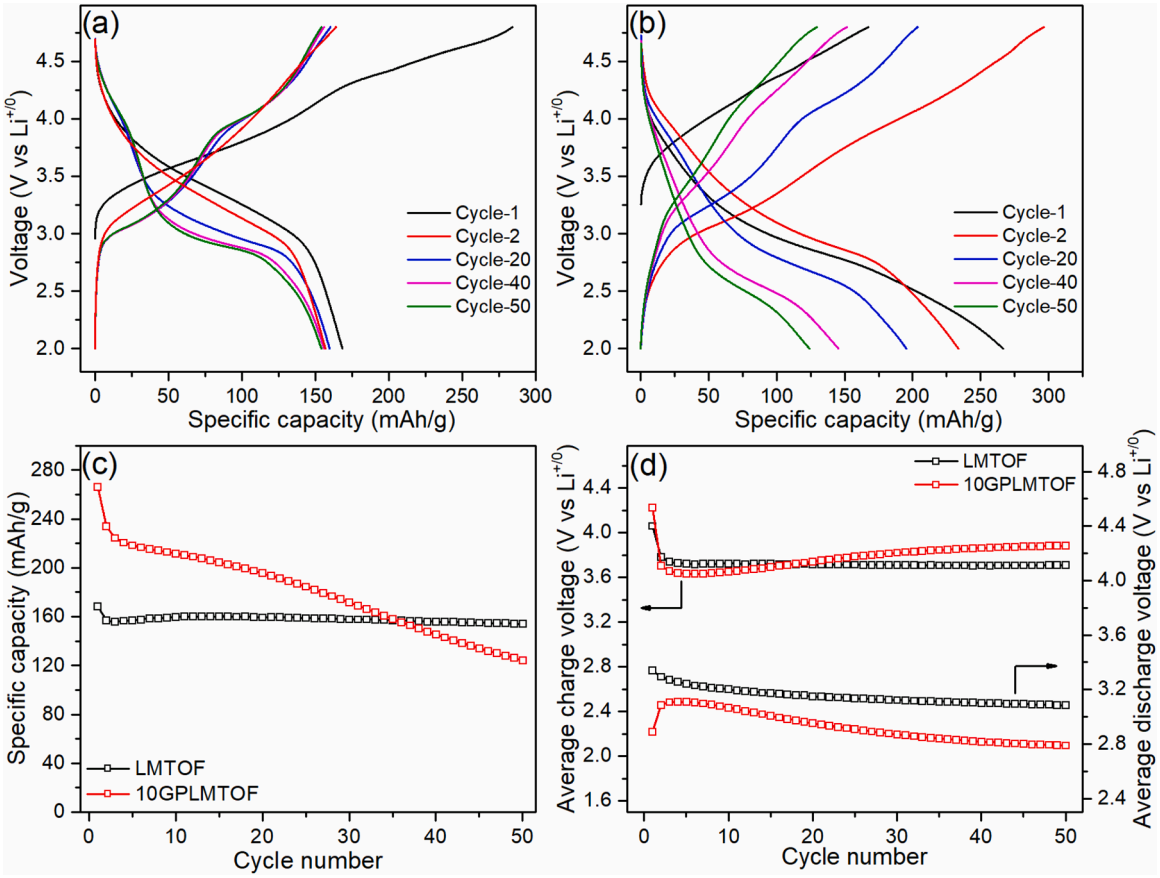

Fig. 3. Galvanostatic charge–discharge profiles of (a) LMTOF and (b) 10GPLMTOF at current density of 20 mA/g. (c) Galvanostatic cycling performance of LMTOF and 10GPLMTOF at 20 mA/g. (d) Average charge and discharge voltages of LMTOF and 10 GPLMTOF obtained from cycling performance at 20 mA/g.

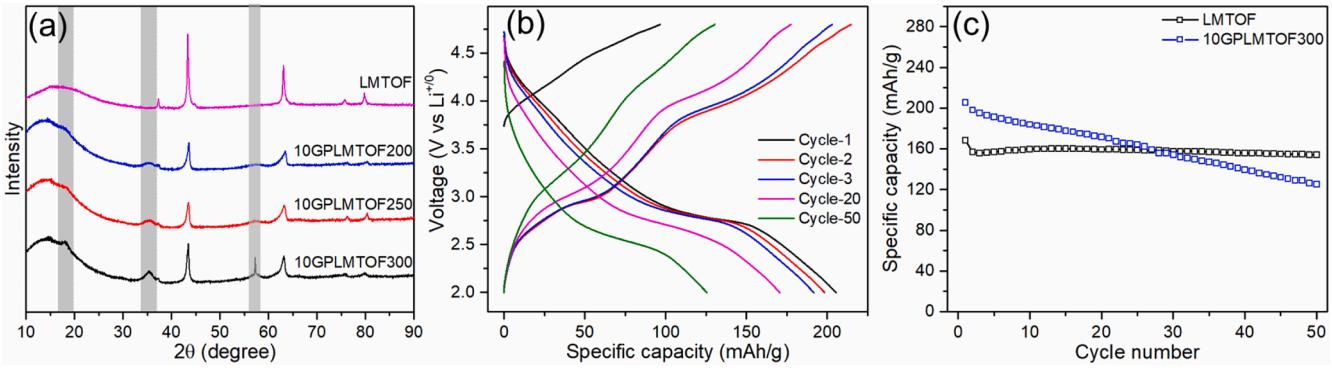

Fig. 4. (a) XRD pattern of LMTOF, 10GPLMTOF200, 10GPLMTOF250 and 10GPLMTOF300. (b) Galvanostatic charge–discharge profiles of 10GPLMTOF300, and (c) galvanostatic cycling performance of LMTOF, and 10GPLMTOF300.

compared to the 10GPLMTOF200 and 10GPLMTOF250. The electrochemical performance of 10GPLMTOF300 was further investigated in Li-metal half-cells. Fig. 4b displays the galvanostatic charge-discharge profiles of the 10GPLMTOF300 at 20 mA/g in the voltage range of 4.8–2.0 V (*vs.* Li/Li^+). 10GPLMTOF300 exhibited an initial discharge capacity of 205 mAh/g at a current density of 20 mA/g, retaining 125 mAh/g after 50 cycles. Moreover, we observed a well-developed plateau at ~3 V in the charge–discharge profiles providing further evidence of the formation of the spinel-like phase. [7] It is likely that the aqueous-medium-based processing leads to Li extraction from LMTOF, which can accelerate the spinel-like phase formation by heat treatment. [33] Although 10GPLMTOF300 exhibited a high initial coulombic efficiency (213 %), and discharge capacities than LMTOF, 10GPLMTOF300 experienced a large polarization and rapid capacity decay (61 % retention after 50 cycles) (Fig. 4b and 4c). The development of electrolytes with improved oxidation limit such as highly concentrated electrolytes [34] may further improve the cycling stability of LMTOF, which needs future studies.

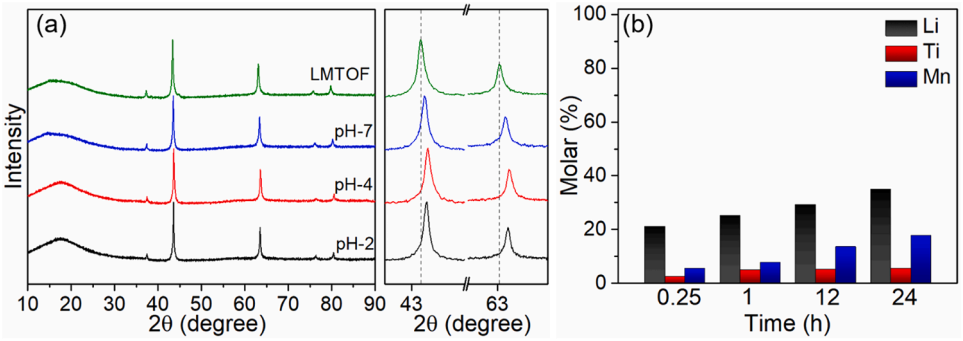

Fig. 5. (a) XRD of LMTOF at various pH (b) ICP-MS analysis of LMTOF dispersed in water at different time intervals at pH 7.

3.4. *Stability of LMTOF in aqueous medium*

To better understand the limitations of the aqueous-solution-based synthesis process, we investigated the stability of LMTOF in the aqueous medium. Fig. 5a shows the XRD patterns of LMTOF after dispersion in aqueous solvents at varied pH levels (pH 7, pH 4, and pH 2) for 1 h. The XRD peaks of LMTOF at ~43° and ~63° shifted to higher two-theta angles, and a lower-pH solvent resulted in more significant XRD peak shifts, indicating that LMTOF degrades faster in acidic environments. Fig. 5b presents the ICP-MS analysis results of a neutral aqueous medium (pH 7) after LMTOF dispersion at varied times. Even after 0.25 h (15 min.), ~20 % of Li (0.24 Li) and ~6 % of Mn (0.0036 Mn) and ~3 % of Ti (0.006 Ti) were leached out from LMTOF. This metal dissolution into aqueous medium becomes more substantial as the time increases up to 24 h with a maximum of 35 % (0.42 Li), 18 % (0.11 Mn), and 6 % (0.012 Ti) from LMTOF.

We also found that the pH level of the aqueous solution after LMTOF dispersion increases substantially up to > pH 10, which agrees well with a recent work by Lee and his colleagues. [35] This implies that Li^+/H^+ exchange reaction occurs between LMTOF and aqueous media as follows:

$$Li^+(\text{in LMTOF}) + H^+(aq) + OH^-(aq) \rightarrow H^+(\text{in LMTOF}) + Li^+(aq) + OH^-(aq) \quad (1)$$

The reaction above indicates that LMTOF can consume H^+ from aqueous media, which results in excess OH^- in the solution (increasing pH level). This reaction mechanism can also explain our observation that an acidic environment accelerates Li ion dissolution as shown in Fig. 1 and Fig. 5. Higher activity of H^+ in an acidic environment shifts the reaction (1) to the right. Similarly, a very recent study by Lun and his colleagues confirms Li^+/H^+ exchange reaction can occur between a DRX compound and an acidic solution. [36] Compared to the conventional layered oxides such as $LiCoO_2$ or $LiNi_xMn_yCo_zO_2$, DRX compounds contain higher Li concentrations in a formula unit and higher Li chemical potential. This implies that Li ions in DRX are energetically less stable than the Li ions in layered oxides. This makes Li^+/H^+ exchange between DRX compounds and aqueous media more thermodynamically favorable compared to the conventional layered oxides. Notably, this study also found that Mn and Ti ions are extracted from LMTOF in aqueous media by characterizing the processing solutions after LMTOF dispersion using ICP-MS as shown in Fig. 5b.

In summary, our findings demonstrate that the LMTOF is unstable in an aqueous medium, and substantial Li^+/H^+ exchange and transition metal dissolution occur when LMTOF is dispersed in aqueous media for the carbon coating process. Therefore, limiting the synthesis reaction time is one important parameter if using an aqueous medium for the synthesis processing, and we believe finding alternative processing media or conditions that do not degrade DRX compounds remains an important challenge.

We further evaluated the electrochemical performance of LMTOF powder after dispersion in an aqueous solution at pH 7 without rGO wrapping (denoted as LMTOF-W) in Li-metal half-cells. Figures S4a-b exhibit the galvanostatic charge-discharge profiles and cycling performance of LMTOF-W in comparison with pristine LMTOF at 20 mA/g in the voltage range of 4.8–2.0 V (*vs.* Li/Li^+). LMTOF-W shows the characteristic charge-discharge behavior of DRX cathodes with a slightly higher initial discharge capacity of 189 mAh/g than the pristine LMTOF (168 mAh/g). While we do not fully understand the origin of a higher initial discharge capacity of the LMTOF-W than the pristine LMTOF, we speculate that the structure change of LMTOF induced by water treatment may promote the Li intercalation kinetics. One possibility is that the Li extraction or Li^+/H^+ exchange by the water treatment could lead to the spinel-like nano-domain formation, which has faster Li diffusion kinetics. [36,37] However, the LMTOF-W shows a relatively rapid capacity decay (87 % retention after 50 cycles) compared to the pristine LMTOF, which retains 90 % of its initial discharge capacity after 50 cycles. We expect that the structure change induced by water treatment harms the structural stability of LMTOF during repeated Li extraction and reinsertion, which may require future studies.

Interestingly, 10GPLMTOF shows even more accelerated capacity degradation compared to LMTOF-W. Notably, the rGO introduced in this work is expected to contain residual functional groups because we could not apply an additional thermal reduction process to avoid the transformation of DRX to the spinel-like phase as shown in Fig. 4a. As we discussed in the previous section, the residual functional groups in the rGO not only decrease electrical conductivity but also provide catalytic sites, which might accelerate electrolyte decomposition. [32] As a result, the residual functional groups in rGO can increase polarization and degrade cycling performance. In this respect, we propose two potential research directions: (i) The use of graphene sheets or carbon flakes with much reduced functional groups are required. However, those graphene sheets or carbon flakes are in general not dispersible in polar solvents such as aqueous media. Therefore, non-polar solvents may need to be applied. (ii) The reduction process of graphene oxide sheets without damaging DRX compounds needs to be established.

4. Conclusion

In this work, we demonstrated the solution-based synthesis for achieving a uniform rGO wrapping on the surface of LMTOF particles using an electrostatic interaction between the negatively charged rGO and positively charged LMTOF particles. Although the rGO wrapping on

LMTOF particles was achieved, the composite underwent degradation during the synthesis process in an aqueous medium. In particular, (1) we found that the LMTOF particles are not stable in aqueous media: Li^+/H^+ exchange and TM dissolution were confirmed when the LMTOF particles are dispersed in aqueous media. (2) The post-annealing process to remove residual functional groups of rGO results in phase transformation of the DRX to spinel-like phase because of the Li loss from the DRX compound in the synthesis step using aqueous media. Therefore, searching for alternative solvents or conditions to process rGO or carbon coating on DRX compounds without Li^+/H^+ exchange and TM dissolution is needed.

CRediT authorship contribution statement

Venkata Sai Avvaru: Writing – review & editing, Writing – original draft, Validation, Methodology, Investigation, Conceptualization. **Mateusz Zuba:** Writing – review & editing, Investigation, Data curation. **Beth L. Armstrong:** Writing – review & editing, Investigation, Data curation. **Shilong Wang:** Writing – review & editing, Investigation, Data curation. **Dong-Min Kim:** Writing – review & editing, Investigation, Data curation. **Isik Su Buyuker:** Formal analysis, Data curation. **Carrie Siu:** Formal analysis, Data curation. **Brett A Helms:** Writing – review & editing, Supervision. **Ozgenur Kahvecioglu:** Writing – review & editing, Supervision. **Haegyeom Kim:** Writing – review & editing, Writing – original draft, Visualization, Supervision, Investigation, Funding acquisition, Conceptualization.

Declaration of competing interest

The authors declare the following financial interests/personal relationships which may be considered as potential competing interests: B. A.H. has a financial interest in Sepion Technologies and Cyklos Materials. If there are other authors, they declare that they have no known competing financial interests or personal relationships that could have appeared to influence the work reported in this paper.

Acknowledgments

This work was supported by the Assistant Secretary for Energy Efficiency and Renewable Energy, Vehicle Technologies Office, of the U.S. Department of Energy under Contract DEAC02–05CH11231 (DRX+ program). D.M. K. and B.A.H. acknowledge support for this work from the Silicon Anode Seedling Project from the U.S. Department of Energy's Vehicle Technologies Office.

Supplementary materials

Supplementary material associated with this article can be found, in the online version, at doi:10.1016/j.electacta.2024.145302.

Data availability

Data will be made available on request.

References

[1] R. Chen, C.L.A. Leung, C. Huang, Exploring the properties of disordered rocksalt battery cathode materials by advanced characterization, Adv. Funct. Mater. (2024) 2308165.
[2] R. Clément, Z. Lun, G. Ceder, Cation-disordered rocksalt transition metal oxides and oxyfluorides for high energy lithium-ion cathodes, Energy Environ. Sci. 13 (2019) 345–373.
[3] J. Qian, Y. Ha, K.P. Koirala, D. Huang, Z. Huang, V.S. Battaglia, C. Wang, W. Yang, W. Tong, Toward stable cycling of a cost-effective cation-disordered rocksalt cathode via fluorination, Adv. Funct. Mater. 33 (2023) 2205972.
[4] M. Wang, X. Chen, H. Yao, G. Lin, J. Lee, Y. Chen, Q. Chen, Research progress in lithium-excess disordered rock-salt oxides cathode, Energy Environ. Mater. 5 (2022) 1139–1154.
[5] D. Chen, J. Ahn, G. Chen, An overview of cation-disordered lithium-excess rocksalt cathodes, ACS Energy Lett. 6 (2021) 1358–1376.
[6] N. Yabuuchi, M. Takeuchi, M. Nakayama, H. Shiiba, M. Ogawa, K. Nakayama, T. Ohta, D. Endo, T. Ozaki, T. Inamasu, K. Sato, S. Komaba, High-capacity electrode materials for rechargeable lithium batteries: Li_3NbO_4-based system with cation-disordered rocksalt structure, Proc. Natl Acad. Sci. USA 112 (2015) 7650–7655.
[7] Z. Cai, B. Ouyang, H.M. Hau, T. Chen, R. Giovine, K.P. Koirala, L. Li, H. Ji, Y. Ha, Y. Sun, J. Huang, Y. Chen, V. Wu, W. Yang, C. Wang, R.J. Clément, Z. Lun, G. Ceder, In situ formed partially disordered phases as earth-abundant Mn-rich cathode materials, Nat Energy 9 (2024) 27–36.
[8] M. Su, Y. Chen, H. Liu, J. Li, K. Fu, Y. Zhou, A. Dou, Y. Liu, Storage degradation mechanism of layered Ni-rich oxide cathode material $LiNi_{0.8}Co_{0.1}Mn_{0.1}O_2$, Electrochim. Acta 422 (2022) 140559.
[9] J.H. Yang, H. Kim, G. Ceder, Insights into layered oxide cathodes for rechargeable batteries, Molecules 26 (2021) 3173.
[10] H. Li, R. Fong, M. Woo, H. Ahmed, D.H. Seo, R. Malik, J. Lee, Toward high-energy Mn-based disordered-rocksalt Li-ion cathodes, Joule 6 (2022) 53–91.
[11] R. Fong, N. Mubarak, S.W. Park, G. Lazaris, Y. Liu, R. Malik, D.H. Seo, J. Lee, Redox engineering of Fe-rich disordered rock-salt Li-Ion Cathode materials, Adv. Energy Mater (2024) 2400402.
[12] J. Kim, Y. Shin, B. Kang, A new class of high-capacity Fe-based cation-disordered oxide for li-ion batteries: li-Fe-Ti-Mo oxide, Adv. Sci. 10 (2023) 2300615.
[13] L. Li, Z. Lun, D. Chen, Y. Yue, W. Tong, G. Chen, G. Ceder, C. Wang, Fluorination-enhanced surface stability of cation-disordered rocksalt cathodes for Li-Ion batteries, Adv. Funct. Mater. 31 (2021) 2101888.
[14] J. Ahn, D. Chen, G. Chen, A fluorination method for improving cation-disordered rocksalt cathode performance, Adv. Energy Mater 10 (2020) 2001671.
[15] Z. Lun, B. Ouyang, D.H. Kwon, Y. Ha, E.E. Foley, T.Y. Huang, Z. Cai, H. Kim, M. Balasubramanian, Y. Sun, J. Huang, Y. Tian, H. Kim, B.D. McCloskey, W. Yang, R.J. Clément, H. Ji, G. Ceder, Cation-disordered rocksalt-type high-entropy cathodes for Li-ion batteries, Nat. Mater. 20 (2021) 214–221.
[16] J. Lee, C. Wang, R. Malik, Y. Dong, Y. Huang, D.H. Seo, J. Li, Determining the criticality of Li-excess for disordered-rocksalt Li-Ion battery cathodes, Adv. Energy Mater 11 (2021) 2100204.
[17] S. Patil, K.P. Koirala, M.J. Crafton, G. Yang, W.Y. Tsai, B.D. McCloskey, C. Wang, J. Nanda, E.C. Self, Enhanced electrochemical performance of disordered rocksalt cathodes enabled by a graphite conductive additive, ACS Appl. Mater. Interfaces 15 (2023) 39253–39264.
[18] A. Outka, H.P. Ho, W.C.H. Kuo, Y. Wang, B. Raji-Adefila, S. Sainio, D. Nordlund, J. Watt, J.H. Wang, D. Chen, Electron localization in cation-disordered rock salt electrodes, ACS Energy Lett 9 (2024) 1863–1870.
[19] J. Ahn, R. Giovine, V.C. Wu, K.P. Koirala, C. Wang, R.J. Clément, G. Chen, Ultrahigh-capacity rocksalt cathodes enabled by cycling-activated structural changes, Adv. Energy Mater 13 (2023) 2300221.
[20] D. Chen, J. Ahn, E. Self, J. Nanda, G. Chen, Understanding cation-disordered rocksalt oxyfluoride cathodes, J. Mater. Chem. A 9 (2021) 7826–7837.
[21] H. Chung, Z. Lebens-Higgins, B. Sayahpour, C. Mejia, A. Grenier, G.E. Kamm, Y. Li, R. Huang, L.F.J. Piper, K.W. Chapman, J.M. Doux, Y.S. Meng, Experimental considerations to study Li-excess disordered rock salt cathode materials, J. Mater. Chem. A 9 (2021) 1720–1732.
[22] J. Xu, S. Patil, K.P. Koirala, W. Chen, A. Campos-Mata, C. Wang, S. Roy, J. Nanda, P.M. Ajayan, Enhancing the electrode gravimetric capacity of $Li_{1.2}Mn_{0.4}Ti_{0.4}O_2$ cathode using interfacial carbon deposition and carbon nanotube-mediated electrical percolation, ACS Appl. Mater. Interfaces 15 (2023) 31711–31719.
[23] C.W. Park, J.H. Lee, J.K. Seo, W.Y. Jo, D. Whang, S.M. Hwang, Y.J. Kim, Graphene collage on Ni-rich layered oxide cathodes for advanced lithium-ion batteries, Nat. Commun. 12 (2021) 2145.
[24] R.A. Ahmed, K.P. Koirala, G.H. Lee, T. Li, Q. Zhao, Y. Fu, L. Zhong, J.D. Daddona, M. Zuba, C. Siu, O. Kahvecioglu, V.S. Battaglia, R.J. Clément, W. Yang, C. Wang, W. Xu, Enhanced electrochemical performance of disordered rocksalt cathodes in a localized high-concentration electrolyte, Adv. Energy Mater. (2024) 2400722.
[25] H. Kim, K.Y. Park, M.Y. Cho, M.H. Kim, J. Hong, S.K. Jung, D.K.C. Roh, P.K. Kang, High-performance hybrid supercapacitor based on graphene-wrapped $Li_4Ti_5O_{12}$ and activated carbon, ChemElectroChem 1 (2014) 125–130.
[26] J.I. Paredes, S. Villar-Rodil, A. Martínez-Alonso, J.M.D. Tascón, Graphene oxide dispersions in organic solvents, Langmuir 24 (2008) 10560–10564.
[27] X. Gong, T. Ngai, Interactions between solid surfaces with preadsorbed poly (ethylenimine) (PEI) Layers: effect of unadsorbed free PEI chains, Langmuir 29 (2013) 5974–5981.
[28] B. Zhou, S. An, D. Kitsche, S.L. Dreyer, K. Wang, X. Huang, J. Thanner, M. Bianchini, T. Brezesinski, B. Breitung, H. Hahn, Q. Wang, Improved performance of high-entropy disordered rocksalt oxyfluoride cathode by atomic layer deposition coating for Li-Ion batteries, Small Struct 5 (2024) 2400005.
[29] T. Mabokela, A.C. Nwanya, M.M. Ndipingwi, S.T. Yussuf, P.I. Ekwere, O.V. Uhuo, C.O. Ikpo, K.D. Modibane, E.I. Iwuoha, Nanostructured europium-doped layered lithium manganese oxide as a prospective cathode material for aqueous lithium-ion battery, Electrochim. Acta 441 (2023) 141865.
[30] L. Sun, L. Wang, C. Tian, T. Tan, Y. Xie, K. Shi, M. Li, H. Fu, Nitrogen-doped graphene with high nitrogen level via a one-step hydrothermal reaction of graphene oxide with urea for superior capacitive energy storage, RSC Adv. 2 (2012) 4498–4506.
[31] P. Chamoli, M.K. Das, K.K. Kar, Urea-assisted low temperature green synthesis of graphene nanosheets for transparent conducting film, J. Phys. Chem. Solids 113 (2018) 17–25.
[32] C. Su, K.P. Loh, Carbocatalysts: Graphene Oxide and Its Derivatives, Acc. Chem. Res. 46 (2013) 2275–2285.

[33] S. Choi, A. Manthiram, Factors Influencing the layered to spinel-like phase transition in layered oxide cathodes, J. Electrochem. Soc. 149 (2002) A1157.
[34] N. Shimada, Y. Ugata, S. Nishikawa, D. Shibata, T. Ohta, N. Yabuuchi, Improved electrode reversibility of anionic redox with highly concentrated electrolyte solution and aramid-coated polyolefin separator, Energy Adv. 2 (2023) 508–512.
[35] J. Lee, H. Ahmed, M. Woo, N. Dumaresq, P. Lara, N. Brodusch, D.H. Seo, R. Gauvin, G. Demopoulos, Nucleation-promoting and growth-limiting synthesis of disordered rock-salt Li-ion cathode materials, https://doi.org/10.21203/rs.3.rs-5154732/v (2024).
[36] Y. Zhang, H. Chen, R. Yu, W. Yang, J. He, H. Li, X. Sun, Z. Lun, Unlocking fast Li-ion transport in micrometer-sized Mn-based cation-disordered rocksalt cathodes, J. Energy Chem. 99 (2024) 645–653.
[37] H.M. Hau, T. Mishra, C. Ophus, T.Y. Huang, K. Bustilo, Y. Sun, X. Yang, T. Holstun, X. Zhao, S. Wang, Y. Ha, G.H. Lee, C. Song, J. Turner, J. Bai, L. Ma, K. Chen, F. Wang, W. Yang, B.D. McCloskey, Z. Cai, G. Ceder, Earth-abundant Li-ion cathode materials with nanoengineered microstructures, Nat. Nanotechnol. (2024) 1–9.